Mechanical Properties and Performance of a Viscoelastic Low-Frequency Vibration Isolation and Mitigation Device

Chao Xu

College of Civil Engineering, Jiangsu Open University, Nanjing 210019, China. E-mail: xuchaolove11@126.com

Xing-Huai Huang

Shenzhen Research Institute, Southeast University, Nanjing 211189, China.

Teng Ge

College of Civil and Transportation Engineering, Hohai University, Nanjing 210098, China.

Ye-Shou Xu

School of Civil Engineering, Southeast University, Nanjing 211189, China.

(Received 24 December 2024; accepted 14 April 2025)

A viscoelastic (VE) low-frequency vibration isolation and mitigation device is proposed in this paper. The device consists of a VE damper, two oblique springs, and two oblique dampers to achieve low stiffness at the equilibrium position. Property tests on the VE damper, which is the core component of the device, are conducted, and a mathematical model is employed to describe the dynamic properties of the VE damper. The influences of mechanical and structural parameters on the stiffness characteristics of the device are investigated through static analysis. The nonlinear dynamic equations of the vibration isolation system with the proposed device are established. The effects of the system parameters on the frequency-amplitude responses and absolute displacement transmissibility are numerically discussed. The isolation performance of the proposed device is compared with that of the isolator, which only consists of a VE damper. The results show that the VE low-frequency vibration isolation and mitigation device can effectively reduce the initial isolation frequency and broaden the isolation frequency interval. The proposed device can obtain better low-frequency isolation and mitigation performance by reasonably designing the device parameters.

1. INTRODUCTION

Vibration is a common phenomenon in nature and engineering, and most of these vibrations are harmful. For example, the vibrations generated by various disturbance sources, such as the reaction wheels or momentum wheels on spacecraft, seriously affect the observation and imaging accuracy.[1,2] The vibrations generated by manipulating tools can induce irreversible body injury for construction, engineering, agriculture and mining workers.[3,4] The earthquake or wind-induced vibrations often lead to the damage of civil engineering structures.[5,6] The environmental vibrations or vibrations of the machine and equipment will reduce the machining precision.[7,8] Therefore, there is a strong demand for vibration suppression technology in engineering, especially in the field of high-precision instruments such as aircraft, high precision satellite and precision machine tools. The most common vibration suppression method is vibration isolation. It is an effective measure for the suppression of vibration by installing vibration isolation devices between the vibration sources and the sensitive payloads to slow down the transmission of vibration. Vibration isolation devices can be classified into passive vibration isolation devices, active/semi-active vibration isolation devices, and hybrid vibration isolation devices.[9,10] However, active/semi-active and hybrid vibration isolation devices require additional hardware, such as sensors, controllers, actuators and power supplies, which increases the energy consumption and complexity of these devices. These characteristics will limit the applications of the active/semi-active and hybrid vibration isolation devices. Passive vibration isolation devices are widely used in vibration suppression due to their simple construction, not having the above-mentioned disadvantages, and the ability to work stably for a long period of time.[11]

For the traditional linear vibration isolation device, there is a contradiction between the frequency range of isolation and the support capacity. The stiffness of the device should be reduced to achieve the faculty of isolating low-frequency vibration. However, reducing the stiffness of the device will result in a reduction in its support capacity. The vibrations in engineering practice generally contain harmful low-frequency components, such as shock and random vibration loads.[12,13] Therefore, the design of a vibration isolation device that possesses an excellent low-frequency vibration isolation effect and meets the load support requirements has attracted the attention of researchers. Some vibration isolation methodologies have been proposed in recent decades, and the most representative is the quasi-zero-stiffness (QZS) isolator with high static and low dynamic stiffness.[14,15] The QZS isolator has been studied extensively and validated as an effective method for low-frequency vibration isolation. The typical QZS isolator is designed by connecting the negative stiffness element in parallel with a matched positive stiffness element. Then the quasi-zero stiffness is obtained around the equilibrium position. The design of the negative stiffness mechanism is the key to the design of the QZS device. Wang et al.[16] proposed the spring-linkage type QZS device in which the negative stiffness in the vertical direction was obtained by two horizontal springs in a compressed state and the linkages. Zhou et al.[17–19] developed the cam-roller-spring type QZS isolator by adopting the conceptual design of cam–roller–spring mechanisms. The mechanical characteristics of the device were analyzed and, a six degree of freedom vibration isolation platform consisting of the cam-roller-spring type QZS struts was also proposed. Lian et al.[20] proposed a micro-vibration absorber with high static and low dynamic stiffness by designing the shape of the buckled beam. The proposed micro-vibration absorber has a low-frequency vibration absorption effect and multiple working modes in multiple directions. Wu et al.[21] developed a compact arrayed-magnetic-spring with negative stiffness (AMS-NS) by arranging the cuboidal magnets as a rectangular array. The analytical and experiment results show that the proposed AMS-NS possesses high negative stiffness density and can effectively broaden the vibration isolation band. Yan G et al.[22–24] proposed and systematically studied a series of bio-inspired structures for low-frequency vibration isolation by imitating animal's legs and paws. These studies can provide a new approach to designing the low-frequency vibration isolators.

The above-mentioned studies show that the proposed QZS isolators can only work effectively under specific loads and within a limited displacement range. Hence, broadening the low-stiffness displacement range and supporting different loads have recently become critical research topics. Zhao et al.[25,26] modified the QZS device by increasing the number of pairs of oblique springs. Then the low-stiffness displacement range on the premise of satisfying the QZS condition was broadened by optimizing the parameter of the modified device. Similarly, Gatti et al.[27] extended the low-stiffness displacement range of the QZS device by changing the positive stiffness element from a single vertical spring to the combination of two oblique springs. Chen et al.[28] studied the deviation of mass load on the dynamic properties of the QZS isolator. They found that adjusting the positive stiffness configuration can reduce the negative effect of the deviation of mass load on the QZS isolator. Zheng et al.[29] proposed a QZS isolator composed of n series-arranged QZS elements to acquire multiple QZS characteristics. Each QZS element consists of a pair of semicircular arches and a pair of oblique beams and exhibits quasi-zero-stiffness characteristics under various specific loads. QZS isolators are still a hot research topic in low-frequency vibration isolation. Researchers are committed to improving the performance of vibration isolators and have proposed several high-performance vibration isolators.[30–32]

As mentioned above, the negative and positive stiffness properties of isolators are typically achieved through ingenious designs that incorporate mechanical springs and rigid components. Especially for the positive stiffness part, mechanical springs are usually used to support the object to achieve positive stiffness characteristics. Hence, the damping of these isolators is small, and additional damping is usually required to enhance vibration isolation performance. Viscous damping is commonly used in these devices. However, adding viscous damping devices will increase the complexity of the isolator and deteriorate the vibration isolation effect in the high-frequency region.[33]

The viscoelastic (VE) dampers are utilized as damping devices in building structures, bridges, vehicles, and mechanical equipment due to the excellent energy dissipation capacity, simple fabrication, and low cost.[34–38] To promote the application and development of VE damping technology in vibration control, a number of experimental and theoretical studies on VE dampers have been conducted.[39–42] However, there are few studies on suppressing low-frequency vibration by using VE devices. Liu et al.[43] studied the characteristics of a QZS isolator by using the VE damper to provide damping and the results showed that optimizing the damping ratio can obtain superior isolation performance both at the resonant frequency and high- frequency region. Hence, the principle of quasi-zero stiffness can be adopted to improve the capacity for suppressing the low-frequency vibration of VE vibration isolation devices. Based on this idea, a new vibration isolation and mitigation device to reduce low-frequency vibration by combining the negative stiffness structure and VE damper, will be designed in this paper.

This study proposes a VE low-frequency vibration isolation and mitigation device by connecting the VE damper in parallel with two oblique springs and dampers. Firstly, the design of the proposed device is introduced. In this part, the VE damper as the core component of the device is investigated experimentally and theoretically. Property tests on the VE damper under different excitations are conducted, and a mathematical model is adopted to describe the dynamic properties of the VE damper. Then, the mechanical characteristics of the device are studied, where the effects of the system parameters on the static properties and dynamic responses are discussed in detail. Finally, the vibration isolation performances of the VE low-frequency vibration isolation and mitigation device are analyzed and discussed.

2. DESCRIPTION OF THE VE LOW-FREQUENCY VIBRATION ISOLATION AND MITIGATION DEVICE

2.1. Design of the Device

The VE low-frequency vibration isolation and mitigation device is shown in Fig. 1(a). The device was composed of two oblique springs, two oblique dampers, and a VE damper. The VE damper was mounted vertically to support the isolated object. The two oblique springs had the same length and stiffness and were assembled symmetrically. One end of the oblique spring was hinged on the base frame, and the other end was hinged on the loading support. Also, the two identical linear dampers were assembled symmetrically, and the ends of the damper were hinged on the base frame and loading support, respectively. It should be noted that when the isolated object was installed, the oblique springs and dampers are in a horizontal position, and the oblique springs were in a compressed state. This position was also known as the static equilibrium position. When the isolated object moved vertically around the

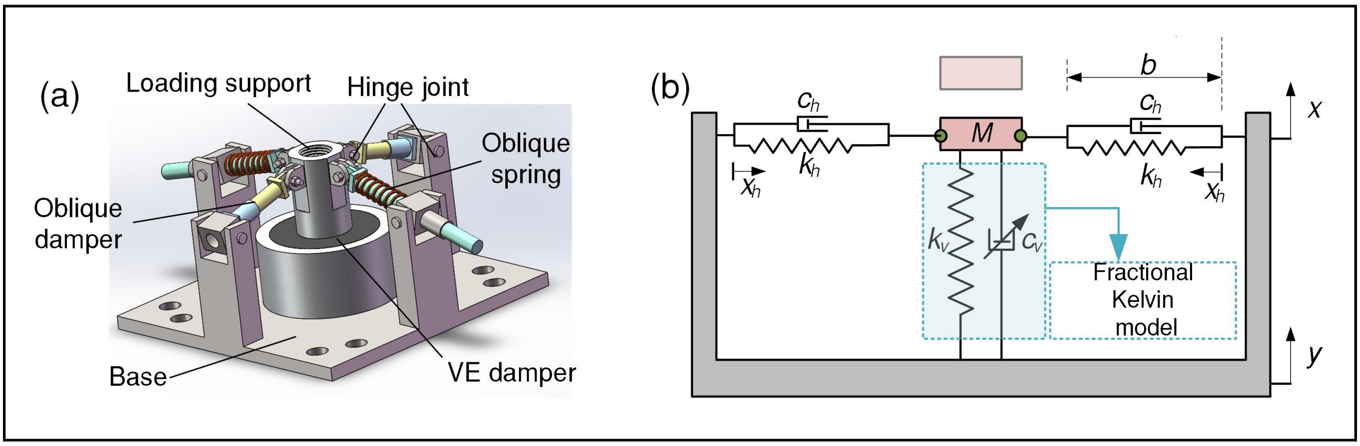

Figure 1. The physical model (a) and schematic diagram (b) of the VE low-frequency vibration isolation and mitigation device.

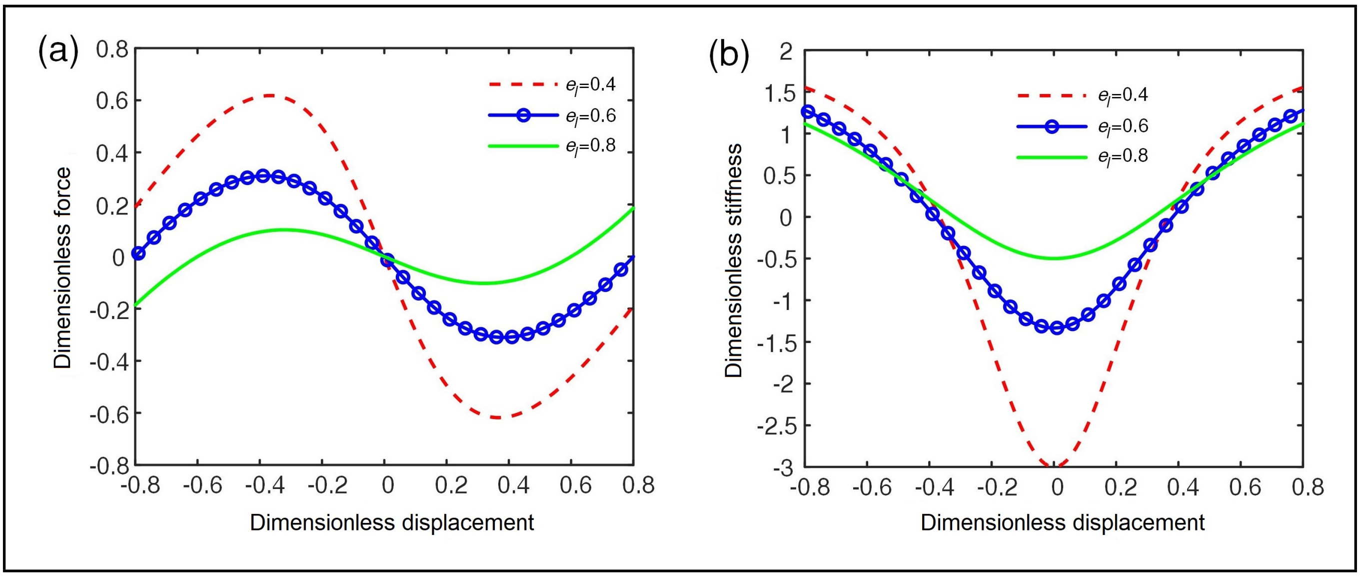

Figure 2. Dimensionless force (a) and dimensionless stiffness (b) for different e_l.

static equilibrium position, the oblique springs remain compressed and provide negative stiffness to the device. The VE damper provides positive stiffness and vertical damping to the device.

2.2. The Negative Stiffness Structure

The negative stiffness structure was considered as in Fig. 1(a), but the VE damper and oblique dampers were removed. When the isolated object moves vertically from the static equilibrium position, the oblique springs remain compressed and generate vertical restoring force acting on the isolated object. The restoring force of the system can be derived as:

$$f = 2k_h \left(1 - \frac{L_0}{\sqrt{(b - x_h)^2 + x^2}}\right) x; \tag{1}$$

where the k_h is the stiffness of the oblique spring, L_0 is the original length of the oblique spring, x was the displacement of the isolated object from the static equilibrium position, b was the length when oblique springs were in the horizontal position and the level adjustment devices were not adjusted, x_h was the adjusted displacement generated by level adjustment devices in horizontal direction.

By using $L_{h0} = b - x_h$, $\hat{f} = \frac{f}{k_h L_0}$, $\hat{x} = \frac{x}{L_0}$, $e_l = \frac{L_{h0}}{L_0}$, the Eq. (1) can be rewritten in non-dimensional form:

$$\hat{f} = 2\left(1 - \frac{1}{\sqrt{e_l^2 + \hat{x}^2}}\right)\hat{x}. \tag{2}$$

To study the structural parameter e_l on the characteristics of the negative stiffness structure, the relationship curves of the non-dimensional restoring force and stiffness regarding the non-dimensional displacement are shown in Figs. 2(a and b). As e_l increased, the stiffness of the structure increased near the static equilibrium position, which means the negative stiffness decreased. Therefore, the stiffness of the negative stiffness structure can be adjusted by changing the length of the oblique springs in horizontal position.

2.3. The Mechanics Characteristics of the // VE Damper

The VE damper was adopted to support the isolated object and provide positive stiffness to the device. Also, the VE damper had excellent energy dissipation capacity and can provide damping in the vertical direction. Many studies show that the mechanical properties of VE dampers are complex and can be affected by excitation frequency, excitation amplitude, and ambient temperature. Therefore, in this part, property tests on

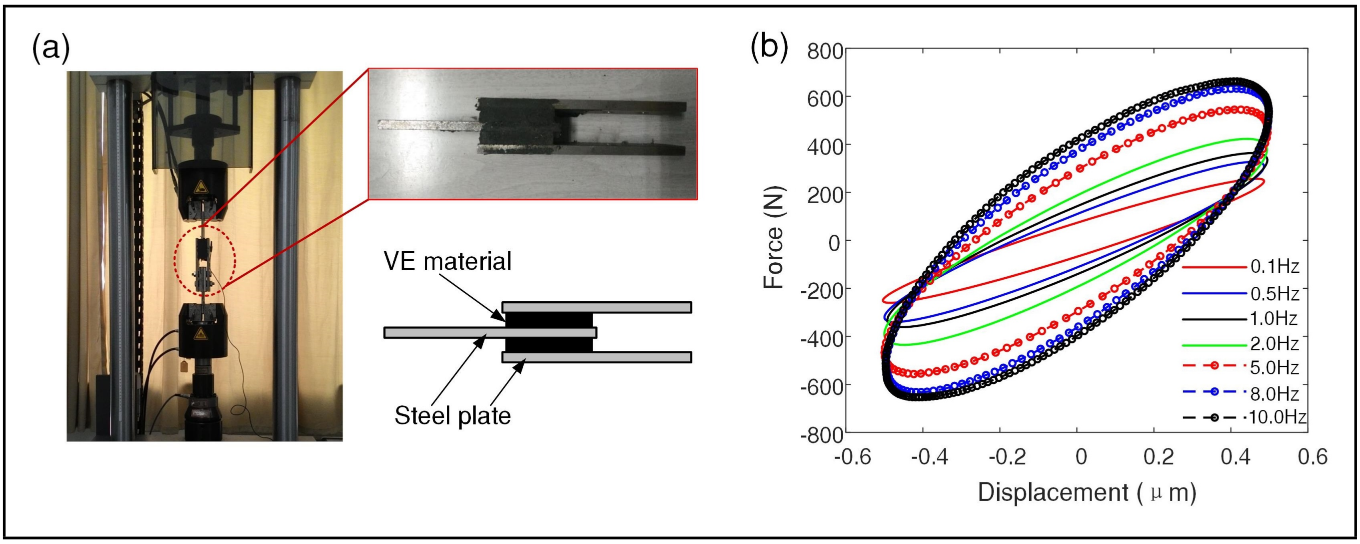

Figure 3. Performance tests on VE damper (a) and the hysteresis curves at different frequencies (b).

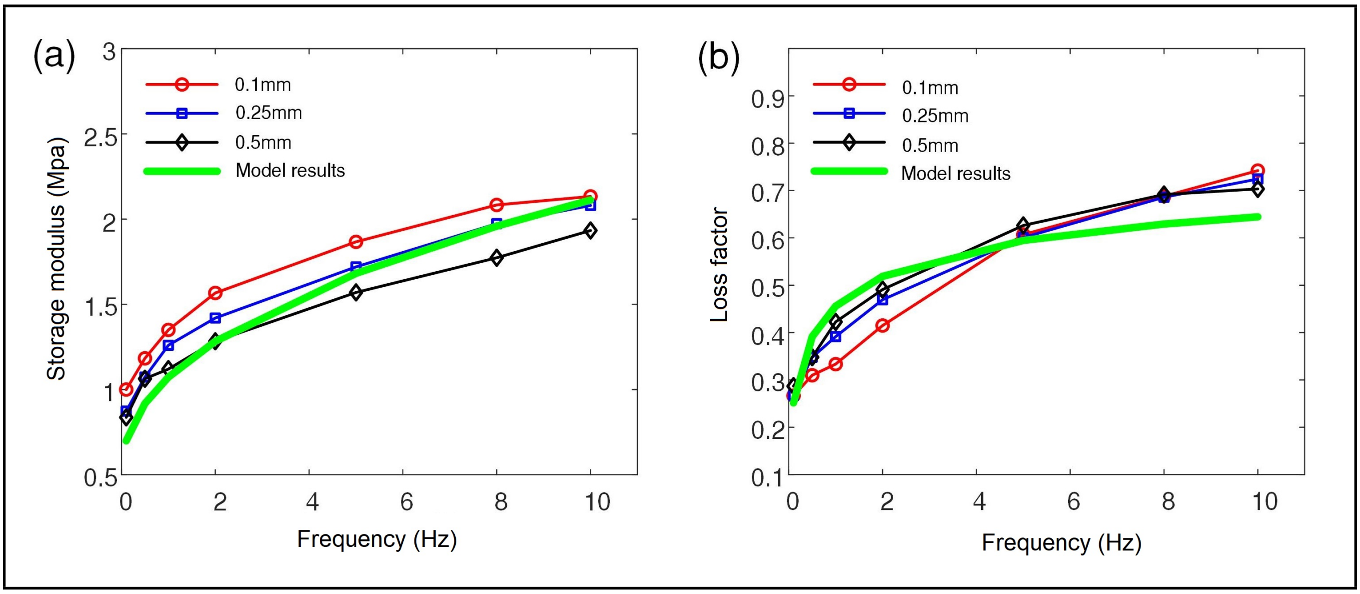

Figure 4. Comparison on experimental results and model calculation results under different frequencies: (a) storage modulus and (b) loss factor.

the VE damper at different frequencies and displacement amplitudes are conducted, and a mathematical model is adopted to describe the dynamic properties of the VE damper.

2.3.1. Tests on the VE Damper

The VE damper tested in this paper is shown in Fig. 3(a), which was manufactured by vulcanization bonding two VE layers between a middle steel plate and two constrained steel plates. The VE material was based on the Nitrile Butadiene Rubber. The performance tests on the VE damper had been carried out in a servo-hydraulic testing machine, as shown in Fig. 3(a). During the tests, the machine was controlled through displacement control mode. Several cycles of sinusoidal excitation with a fixed displacement amplitude and excitation frequency were applied on the VE damper to obtain steady force-displacement hysteresis curves in each test condition. The excitation displacement amplitudes were 0.1 mm, 0.25 mm, and 0.5 mm, and at each amplitude, the excitation frequencies were 0.1 Hz, 0.5 Hz, 1 Hz, 2 Hz, 5 Hz, 8 Hz, and 10 Hz. The tests were conducted at a room temperature of about $12°$C.

The force-displacement hysteresis curves can be obtained at each test, and several representative hysteresis curves are plotted in Fig. 3(b). The hysteresis curves were fully elliptical, and the slope increases with increasing excitation frequency, which indicates that the VE damper has good energy dissipation capacity and that its dynamic properties are significantly affected by frequency.

The critical performance parameters of the VE damper can be obtained from the hysteresis curves,[44] such as storage modulus G_1 and loss factor η. The storage modulus and the loss factor of the VE damper at different frequencies are depicted in Figs. 4(a and b). It can be obviously seen that the storage modulus and the loss factor increase with increasing frequency, while the effect of displacement amplitude on the dynamic properties of the VE damper was slight. The equivalent stiffness k_{eq} and the equivalent damping c_{eq}, which can characterize the mechanical properties of the VE damper at different frequencies, are depicted in Fig. 5. The equivalent stiffness increased with increasing frequency, while the equivalent damping sharply decreased with increasing frequency. The effects of displacement amplitude on the equivalent stiffness and equivalent damping are slight.

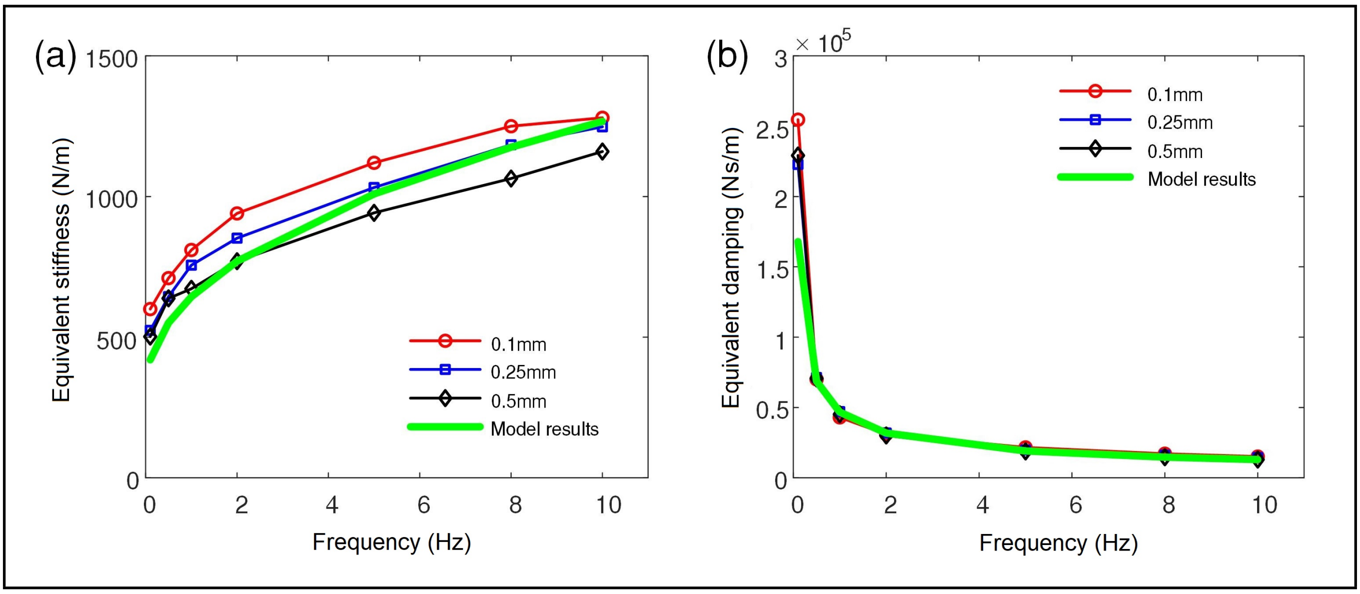

Figure 5. Comparison on experimental results and model calculation results under different frequencies: (a) equivalent stiffness and (b) equivalent damping.

2.3.2. The Mathematical Model of the VE Damper

The experimental results show that the dynamic properties of the VE damper are affected by excitation frequency. To describe the dynamic properties of the VE damper, some mathematical models have been proposed, such as the Maxwell model, Kelvin model, standard solid model, equivalent standard solid model, and fractional derivative model.[45] Among these models, the advantage of the fractional derivative model is its ability to accurately describe the behavior of VE dampers over a wide range of frequencies with fewer constants.[46,47] Hence, the fractional Kelvin model will be adopted to represent the VE damper in this study. In this model, the VE damper is simulated by using fractional calculus and consists of a spring and a dash-pot connected in parallel, as shown in Fig. 1(b).

The constitutive equation of the fractional Kelvin model can be expressed as:

$$f_{ve} = q_0 x(t) + q_1 D^p[x(t)]; \tag{3}$$

where q_0 and q_1 are the coefficients related to the VE materials, p was the fractional order, f_{ve} and $x(t)$ were the restore force and displacement of the VE damper, respectively, $D^p[x(t)]$ was the p-order derivative of $x(t)$ to t, and the Caputo's definition was adopted to define the fractional-order derivative. It should be noted that $0 < p < 1$, while $p = 1$ represented the classical Kelvin model. By transforming Eq. (3) into the frequency domain, the constitutive parameters of this model under sinusoidal excitation can be expressed as:

$$\begin{aligned} G_1 &= q_0 + q_1\omega^p \cos(p\pi/2); \\ G_2 &= q_1\omega^p \sin(p\pi/2); \\ \eta &= \frac{G_2}{G_1} = \frac{q_1\omega^p \sin(p\pi/2)}{q_0 + q_1\omega^p \cos(p\pi/2)}; \end{aligned} \tag{4}$$

where the G_1, G_2 and η was the storage modulus, loss modulus and loss factor of the VE material used in the VE damper, respectively. ω was the excitation frequency.

To verify the accuracy of the mathematical model, the storage modulus G_1 and the loss factor η of the VE material were calculated by Eq. (4) and compared with the test data. The results at different frequencies are also shown in Fig. 4. The numerical results are in good agreement with the experimental results for the storage modulus G_1 and the loss factor η. The maximum errors of the storage modulus G_1 and the loss factor η are 13.64% and 12.51%, respectively. To further verify the availability of the fractional Kelvin model, the equivalent stiffness k_{eq} and the equivalent damping c_{eq} of the VE damper can be calculated by the following equations by referencing to the related literatures:[39,44]

$$\begin{aligned} k_{eq} &= \frac{nn \cdot A_v}{h_v} G_1 = \frac{nn \cdot A_v}{h_v}\left(q_0 + q_1\omega^p \cos\left(\frac{p\pi}{2}\right)\right); \\ c_{eq} &= \frac{nn \cdot A_v}{h_v \omega} G_2 = \frac{nn \cdot A_v}{h_v} q_1 \omega^{p-1} \sin\left(\frac{p\pi}{2}\right); \end{aligned} \tag{5}$$

where nn, A_v and h_v were the number of VE layers, the shear area and the thickness of the VE layer, respectively. These constants are related to the construction of the VE damper. The comparison of the numerical results and experimental results at different frequencies are shown in Fig. 5. The numerical results for the equivalent stiffness and the equivalent damping are in good agreement with the experimental results.

Hence, the fractional Kelvin model can precisely describe the dynamic properties of the VE damper, and will be used to model the VE damper in the low-frequency vibration isolation and mitigation device in the following section.

3. MECHANICAL PROPERTIES OF THE VE LOW-FREQUENCY VIBRATION ISOLATION AND MITIGATION DEVICE

Figure 1(b) shows the schematic diagram of the model of the VE low-frequency vibration isolation and mitigation device. The VE damper was represented by the fractional Kelvin model, which can well describe the effect of the excitation frequency on its properties, as studied in the previous section. In this section, the mechanical characteristics of the VE low-frequency vibration isolation and mitigation device will be studied in detail.

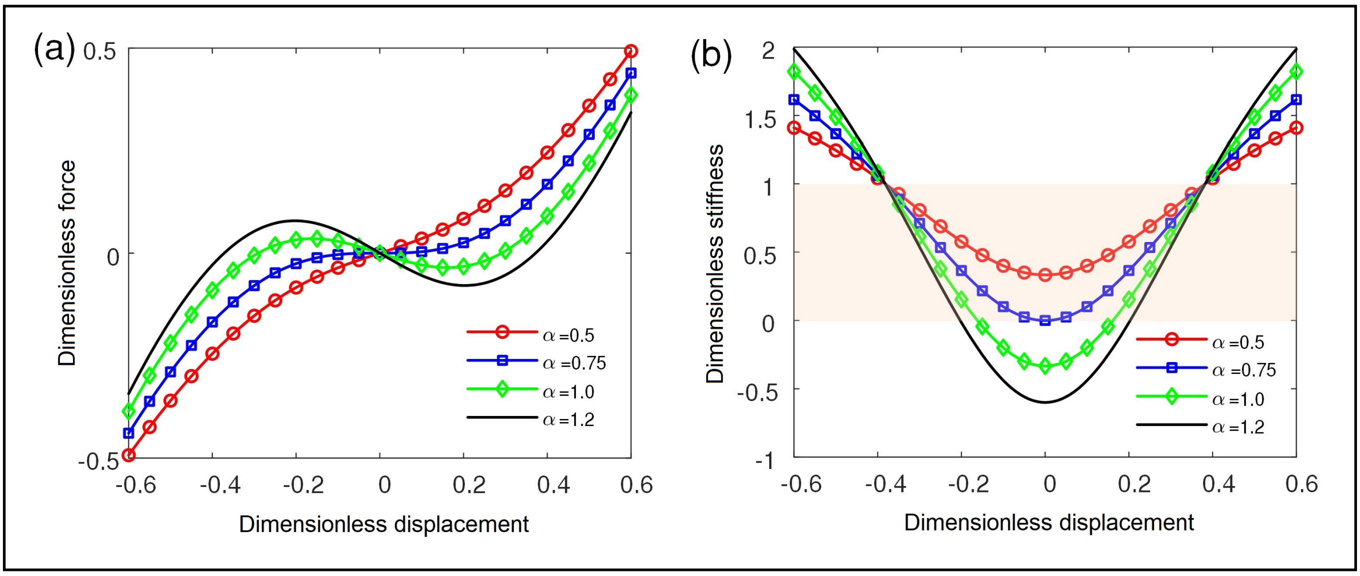

Figure 6. Dimensionless force (a) and dimensionless stiffness (b) for different α and $e_l = 0.6$.

3.1. Static Analysis

As shown in Fig. 1(b), the isolated object is in the static equilibrium position, and the oblique springs are in the horizontal position and compressed. The forces of the oblique springs on the isolated object cancel with each other in the horizontal direction, and the gravity force of the isolated object was supported by the VE damper. When the isolated object moves up or down from the equilibrium position in the vertical direction with displacement x, the restoring force of the device can be written as:

$$F = k_v x + 2k_h \left(1 - \frac{L_0}{\sqrt{L_{h0}^2 + x^2}}\right) x; \tag{6}$$

where k_v was the stiffness provided by the VE damper as shown in Fig. 1.

Let $\alpha = \frac{k_h}{k_v}$ and $\hat{F} = \frac{F}{k_v L_0}$, Eq. (6) can be rewritten in non-dimensional form:

$$\hat{F} = \hat{x} + 2\alpha \left(1 - \frac{1}{\sqrt{e_l^2 + \hat{x}^2}}\right) \hat{x}. \tag{7}$$

The dimensionless stiffness $\hat{K}$ can be obtained by differentiating Eq. (7) with respect to the dimensionless displacement $\hat{x}$:

$$\hat{K} = 1 + 2\alpha \left(1 - \frac{1}{\sqrt{e_l^2 + \hat{x}^2}}\right) + 2\alpha \hat{x}^2 \left(e_l^2 + \hat{x}^2\right)^{-\frac{3}{2}}. \tag{8}$$

According to Eqs. (7) and (8), the dimensionless restoring force and stiffness of the device are related to the stiffness ratio α and the structure parameter e_l. To study the effects of these parameters on the mechanical characteristics of the device, the relationship curves of the dimensionless restoring force and stiffness regarding the dimensionless displacement for various parameters are depicted in Figs. 6 and 7, respectively. It can be seen from Fig. 6 that the stiffness of the device near the equilibrium position decreases as the stiffness ratio α increases when the parameter e_l is constant. The stiffness increases with increasing displacement in the small displacement range. The minimum stiffness achieved at the static equilibrium position changes from positive to negative as the stiffness ratio α increases. When the parameter α is constant, the stiffness increases with increasing parameter e_l as shown in Fig. 7. The stiffness near the equilibrium position changes from negative to positive as the parameter e_l increases.

It is worth noting that the stiffness of the device should be greater than or equal to zero near the equilibrium position. Then, the device can support the isolated object. Also, the stiffness should be less than one near the equilibrium position, which means the stiffness of the proposed device is lower than that without a negative stiffness structure. Hence, the parameters α and e_l needed to be selected appropriately to gain the minimal stiffness (i.e., zero stiffness) at the equilibrium position. By setting Eq. (8) equal to zero at $\hat{x} = 0$, the QZS condition can be determined as:

$$\alpha = \frac{e_l}{2(1 - e_l)}. \tag{9}$$

The relationship curves of the non-dimensional stiffness versus the non-dimensional displacement when the parameters α and e_l satisfy Eq. (9) are depicted in Fig. 8. The stiffness is zero at the equilibrium position. Near the static equilibrium position, the stiffness first decreases and then increases as the parameter α increases. Therefore, to achieve smaller stiffness and a wider low stiffness interval near the equilibrium position, it is necessary to reasonably select parameters α and e_l.

3.2. Dynamic Analysis

3.2.1. Dynamic Modeling

The dynamic equation of the VE low-frequency vibration isolation and mitigation device was formulated, and its dynamic characteristics were analyzed in this section. The schematic diagram of the dynamic model of the device is shown in Fig. 1(b). Considering the base is excited by harmonic excitation displacement $y = Y_0 \cos \omega t$, and the isolated object M moved vertically with displacement x, the dynamic

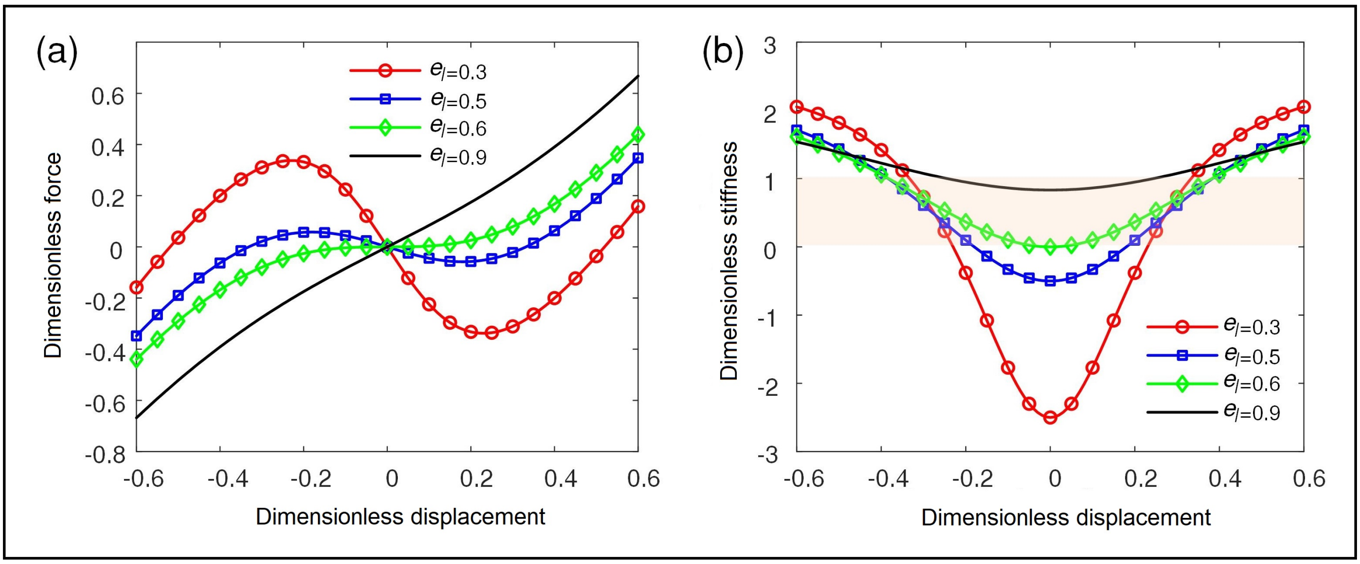

Figure 7. Dimensionless force (a) and dimensionless stiffness (b) for different e_l and $\alpha = 0.75$.

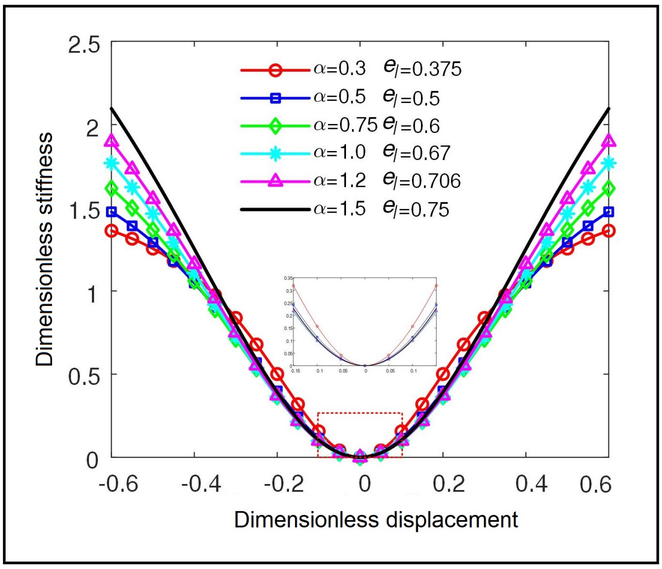

Figure 8. Dimensionless stiffness-displacement curves.

equation of the system can be deduced as follows:

$$M\ddot{x} + k_v(x-y) + 2k_h\left(1 - \frac{L_0}{\sqrt{L_{h0}^2 + (x-y)^2}}\right)(x-y) + c_v D_t^p[x-y] + 2c_h\frac{(x-y)^2(\dot{x}-\dot{y})}{L_{h0}^2 + (x-y)^2} = 0; \tag{10}$$

where c_h and c_v were the damping coefficients of the oblique damper and VE damper, respectively. Let $z = x - y$ be the relative displacement of the isolated object with respect to the base, the dynamic equations can be reformulated as:

$$M\ddot{z} + k_v z + 2k_h\left(1 - \frac{L_0}{\sqrt{L_{h0}^2 + z^2}}\right)z + c_v D_t^p[z] + 2c_h\frac{z^2\dot{z}}{L_{h0}^2 + z^2} = -M\ddot{y}. \tag{11}$$

Let $\omega_n = \sqrt{\frac{k_v}{M}}$, $\zeta_h = \frac{c_h}{2M\omega_n}$, $\zeta_v = \frac{c_v}{2M\omega_n}$, $\hat{Y} = \frac{Y_0}{L_0}$, and $\hat{z} = \frac{z}{L_0}$. Equation (11) can be rewritten in dimensionless form as:

$$\ddot{\hat{z}} + \omega_n\left(1 + 2\alpha\left(1 - \frac{1}{\sqrt{e_l^2 + \hat{z}^2}}\right)\right)\hat{z} + 2\zeta_v\omega_n D_t^p[\hat{z}] + 4\zeta_h\omega_n\frac{\hat{z}^2\dot{\hat{z}}}{e_l^2 + \hat{z}^2} = \hat{Y}_0\omega^2\cos(\omega t). \tag{12}$$

Equation (12) is highly nonlinear and difficult to solve directly. To simplify the subsequent dynamic analysis, the nonlinear restoring force and damping force needed to be approximated. The dimensionless restoring force expressed by Eq. (7) can be approximated by using a third-order Taylor series expansion as:

$$\hat{F}_{app} = \left(1 + 2\alpha - \frac{2\alpha}{e_l}\right)\hat{x} + \alpha e_l^{-3}\hat{x}^3. \tag{13}$$

Similarly, the nonlinear damping ratio can be approximated as $\zeta_{h\,app} = 2\zeta_h\frac{z^2}{e_l^2}$.

The exact and approximate restoring force and damping ratio are shown in Fig. 9. The approximate accuracy is related to the displacement, the approximate restoring force and damping ratio are almost identical with the exact one in a small range of displacement. Thus, the approximate restoring force and damping ratio can be used to replace the exact one for micro-vibration conditions, and Eq. (12) can be rewritten as:

$$\ddot{\hat{z}} + \omega_n^2\eta_1\hat{z} + \omega_n^2\eta_2\hat{z}^3 + 2\zeta_v\omega_n D_t^p[\hat{z}] + 2\zeta_h\omega_n\eta_3\hat{z}^2\dot{\hat{z}} = \hat{Y}_0\omega^2\cos(\omega t); \tag{14}$$

where $\eta_1 = \left(1 + 2\alpha - \frac{2\alpha}{e_l}\right)$, $\eta_2 = \alpha e_l^{-3}$, $\eta_3 = \frac{2}{e_l^2}$.

Here the Caputo's definition is adopted to define the fractional order derivative as:

$$D_t^p[z(t)] = \frac{1}{\Gamma(1-p)}\int_0^1 \frac{z(u)}{(t-u)^p}\,du; \tag{15}$$

where $\Gamma(x)$ is Gamma function satisfying $\Gamma(x+1) = x\Gamma(x)$.

When the system was in steady-state motion, the high-order components of the movement can be neglected, and only the

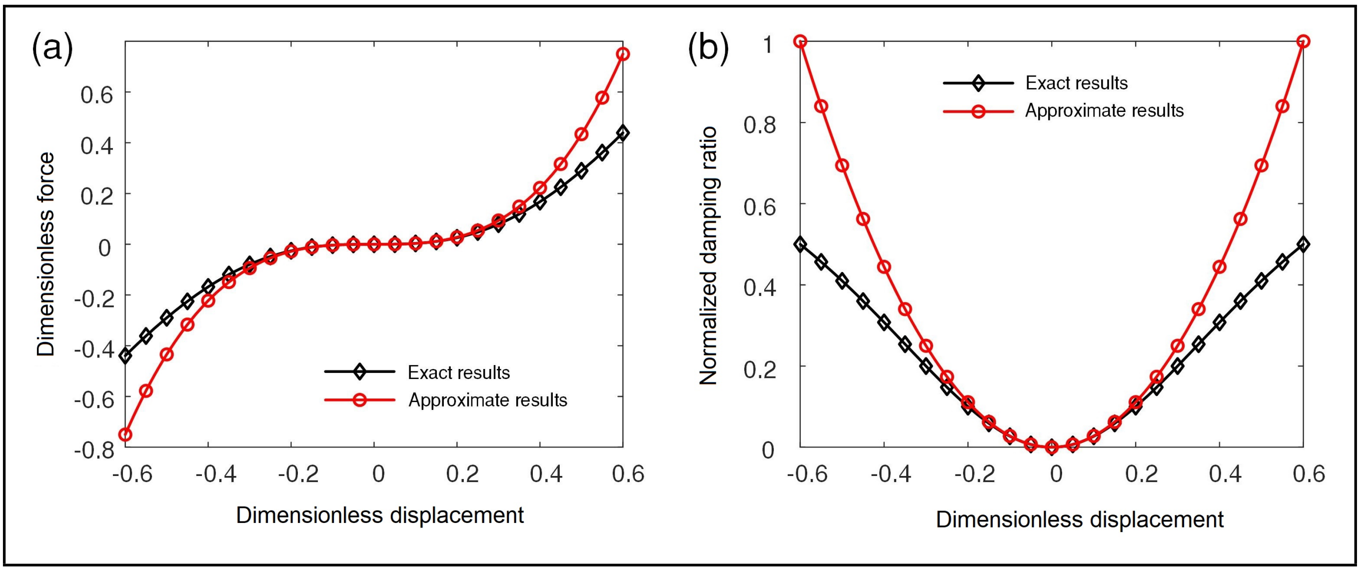

Figure 9. Comparison on exact results and approximate results: (a) dimensionless force and (b) normalized damping.

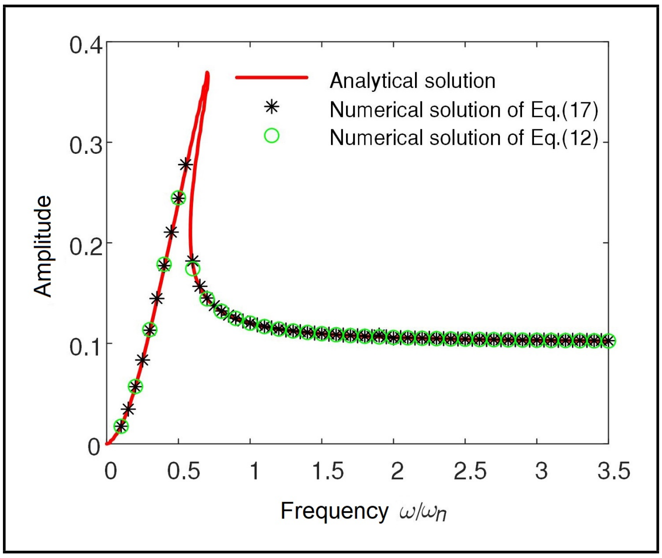

Figure 10. Comparison between the analytical and numerical response amplitudes.

first-order component was considered, then the fractional order derivative in Eq. (14) can be approximated as:[48]

$$D_t^p[z(t)] = \omega^{p-1}\sin\left(\frac{p\pi}{2}\right)\dot{z}(t) + \omega^p\cos\left(\frac{p\pi}{2}\right)z(t). \quad (16)$$

It can be seen from Eq. (16), that the fractional order derivative term exhibits both the damping and stiffness properties, which is consistent with the equivalent stiffness and equivalent damping of VE dampers as analyzed in Section 2.3. Then, Eq. (14) can be rewritten as:

$$\ddot{\hat{z}} + \omega_n^2\eta_1\hat{z} + \omega_n^2\eta_2\hat{z}^3 + 2\zeta_v\omega_n(\theta_1\hat{z} + \theta_2\dot{\hat{z}}) + 2\zeta_h\omega_n\eta_3\hat{z}^2\dot{\hat{z}} = \hat{Y}_0\omega^2\cos(\omega t); \quad (17)$$

where $\theta_1 = \omega^p\cos\left(\frac{p\pi}{2}\right)$, $\theta_2 = \omega^{p-1}\sin\left(\frac{p\pi}{2}\right)$.

To analyze the dynamic characteristics of the device, the approximate analytical solution of Eq. (17) was solved by employing the harmonic balance method,[49] and the amplitude-frequency characteristic equation of the system was derived. Assuming the steady-state response of displacement has the form:

$$\hat{z}(t) = Z_0\cos(\omega t - \phi). \quad (18)$$

It can be substituted in Eq. (17). By setting the coefficient of the same harmonics equal and neglecting the higher order harmonics, one can obtain the following equations:

$$\begin{aligned}
&-\omega^2 Z_0\cos(\phi) + \omega_n^2\eta_1 Z_0\cos(\phi) + \frac{3}{4}\omega_n^2\eta_2 Z_0^3\cos(\phi) + \\
&\quad 2\zeta_v\omega_n\omega\theta_2 Z_0\sin(\phi) + 2\zeta_v\omega_n\theta_1 Z_0\cos(\phi) + \\
&\quad \frac{1}{2}\eta_3\zeta_h\omega_n\omega Z_0^3\sin(\phi) = \hat{Y}_0\omega^2; \\
&-\omega^2 Z_0\sin(\phi) + \omega_n^2\eta_1 Z_0\sin(\phi) + \frac{3}{4}\omega_n^2\eta_2 Z_0^3\sin(\phi) - \\
&\quad 2\zeta_v\omega_n\omega\theta_2 Z_0\cos(\phi) + 2\zeta_v\omega_n\theta_1 Z_0\sin(\phi) - \\
&\quad \frac{1}{2}\eta_3\zeta_h\omega_n\omega Z_0^3\cos(\phi) = 0. \quad (19)
\end{aligned}$$

Then, by eliminating the ϕ with $\sin^2(\phi) + \cos^2(\phi) = 1$, the amplitude-frequency response relationship of the system can be obtained as:

$$\begin{aligned}
&\left(\frac{1}{4}\eta_3^2\zeta_h^2\omega_n^2\omega^2 + \frac{9}{16}\omega_n^4\eta_2^2\right)Z_0^6 + \left(-\frac{3}{2}\omega^2\omega_n^2\eta_2 + \right. \\
&\quad \left.\frac{3}{2}\omega_n^4\eta_1\eta_2 + 3\zeta_v\omega_n^3\eta_2\theta_1 + 2\eta_3\theta_2\zeta_v\zeta_h\omega_n^2\omega^2\right)Z_0^4 + \\
&\quad \left(\omega^4 + \omega_n^4\eta_1^2 + 4\zeta_v^2\omega_n^2\theta_1^2 - 2\omega^2\omega_n^2\eta_1 - 4\zeta_v\omega^2\omega_n\theta_1 + \right. \\
&\quad \left.4\eta_1\zeta_v\omega_n^3\theta_1 + 4\zeta_v^2\omega_n^2\omega^2\theta_2^2\right)Z_0^2 = \hat{Y}_0^2\omega^4. \quad (20)
\end{aligned}$$

The amplitude-frequency response curves as shown in Fig. 10 can be analytically obtained based on Eq. (20). In order to verify the precision of analytical solution as above mentioned, Eq. (12) is solved numerically by employing the fractional order extended state equation method.[50] It can be seen that the analytical results agree well with the numerical results. Also, the approximate equation of the system, as shown in Eq. (17), is solved by employing the Runge–Kutta method, and the results are plotted in Fig. 10. Numerical results of Eq. (12) and Eq. (17) are also in great agreement with each

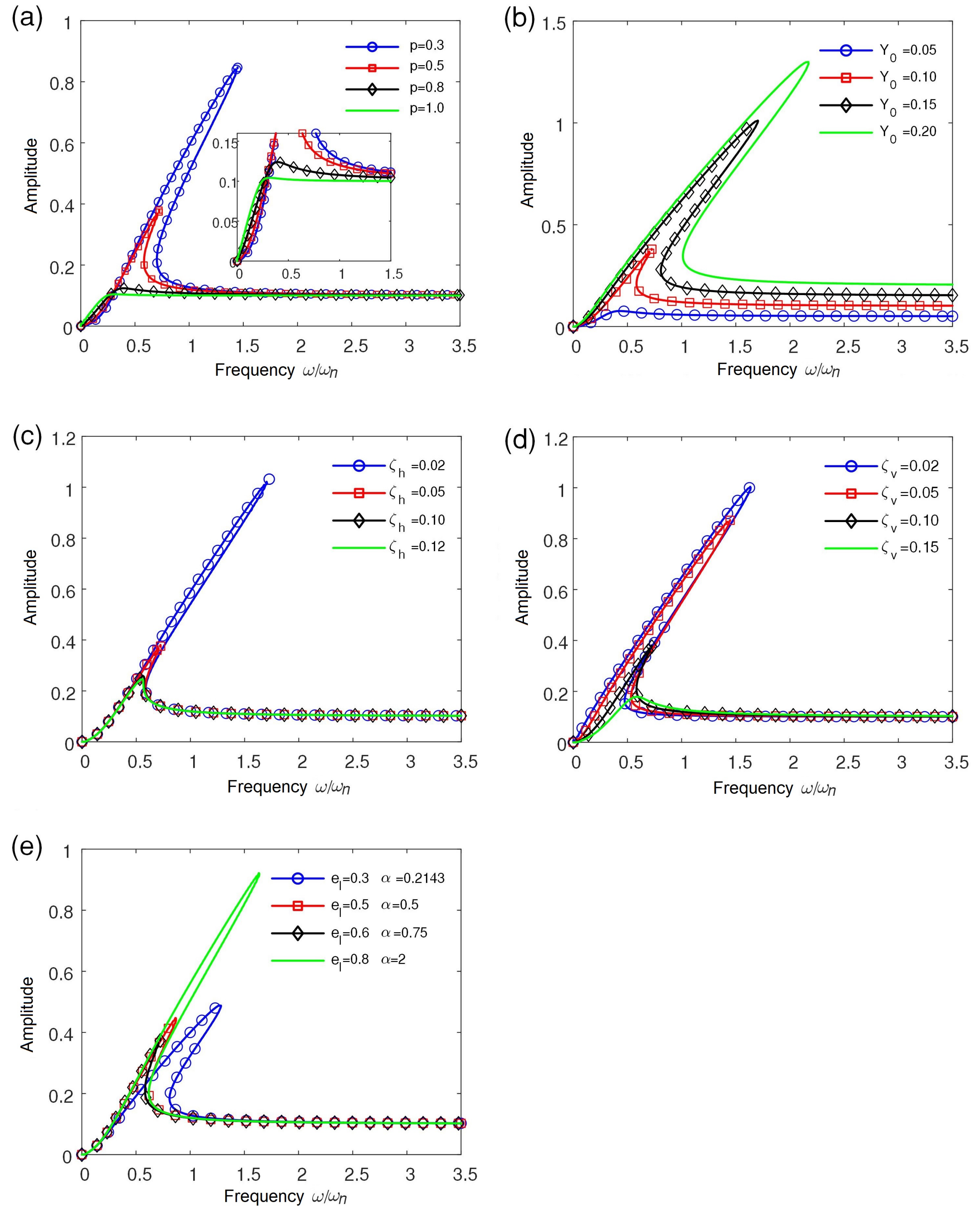

Figure 11. Effects of parameters on dynamic response characteristics: (a) effects of fractional order, (b) effects of excitation amplitude, (c) effects of horizontal damping ratio, (d) effects of vertical damping ratio, and (e) effects of stiffness ratio and structure parameter.

other. Hence, the amplitude-frequency response results can be used to analyze the dynamic characteristics of the system and, both Eq. (12) and Eq. (17) can be used to directly solve the dynamic response of the system.

3.2.2. Effects of Parameters on the Amplitude-Frequency Responses

It can be seen from Eq. (20), that the amplitude-frequency responses are mainly concerned with the excitation displacement amplitude $\hat{Y}_0$, the horizontal damping ratio ζ_h, the vertical damping ratio ζ_v, the fractional order p, the stiffness ratio α and the structure parameter e_l. It should be noted that the stiffness ratio α and the structure parameter e_l need to satisfy Eq. (9) to ensure that the device obtains quasi-zero stiffness characteristics at the equilibrium position. In this section, the numerical analysis method based on Eq. (20) is used to investigate the influences of different $\hat{Y}_0$, ζ_h, ζ_v, p, α and e_l on the amplitude-frequency responses, and the results are depicted in Fig. 11. In the numerical example, the natural frequency ω_n is set to 1, and the other parameters are shown in Table 1.

The influence of the fractional order p on the amplitude-frequency response is plotted in Fig. 11(a). As the fractional order p decreases, the maximum amplitude increases, and the bending degree of the amplitude-frequency curve is more severe. It can be easily explained by Eq. (5) that the smaller the fractional order p is, the smaller the equivalent damping is and the larger the equivalent stiffness is. It is well known that, for a vibration isolation system, the lower stiffness means lower resonance frequency and higher damping means smaller response amplitude.

Figure 11(b) shows the effects of the excitation amplitude on the amplitude-frequency response. As the excitation amplitude increases, the maximum amplitude increases and the amplitude-frequency response curve bends more severely. When the excitation amplitude is small, the jump phenomenon of the amplitude-frequency response curve almost disappears. It means that the device has better vibration isolation performance under small excitation displacements.

Figure 11(c) shows the effects of the horizontal damping ratio on the amplitude- frequency responses. The maximum amplitude decreases rapidly with increasing horizontal damping. Moreover, the horizontal damping ratio almost does not affect the amplitude response outside the resonant frequency range.

Figure 11(d) shows the effects of the vertical damping ratio on the amplitude-frequency responses. The smaller the vertical damping ratio is, the larger the maximum amplitude is. Additionally, the resonance region shifts to the left when the vertical damping ratio decreases. This is because the equivalent damping and the equivalent stiffness become smaller when the damping ratio decreases, which will result in lower resonance frequency and larger response amplitude. These conclusions are the same as the results in the traditional vibration isolation system.

Figure 11(e) shows the effects of the stiffness ratio α and structure parameter e_l on the amplitude-frequency response. Here the α and e_l satisfied the relationship of Eq. (9) to ensure the stiffness of the device at the equilibrium position was zero. Different combinations of α and e_l have a large effect on the amplitude-frequency response. As e_l increases, the maximum amplitude decreases firstly and then increases, and the skeleton of the amplitude-frequency response curve moves to left firstly and then to right. The skeleton of the amplitude-frequency response curve represents the resonance characteristics of the nonlinear vibration isolation system, which is very important for the design of the vibration isolation system. Hence, a reasonable combination of α and e_l need to be selected in the design of the device.

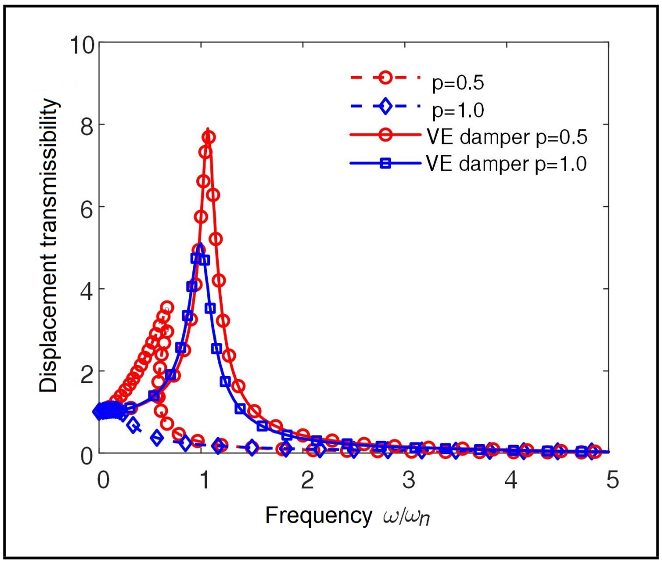

Figure 12. Displacement transmissibility of the proposed device and the VE damper.

4. VIBRATION ISOLATION PERFORMANCE ANALYSES OF THE VE LOW-FREQUENCY VIBRATION ISOLATION AND MITIGATION DEVICE

4.1. Absolute Displacement Transmissibility Analysis

The displacement transmissibility was used as an index to reflect the vibration isolation performance of the system. It was defined as the ratio of the amplitude of the absolute displacement of the isolated object to the amplitude of the base displacement. The absolute displacement transmissibility of the system can be expressed as:

$$T_d = \frac{|z+y|}{|y|} = \frac{\sqrt{Z_0^2 + Y_0^2 + 2Z_0Y_0\cos(\phi)}}{Y_0}. \tag{21}$$

To verify the low-frequency vibration isolation performance of the proposed device, its absolute displacement transmissibility was compared with that of a device without the oblique springs and dampers. It can be seen from Fig. 1, that the vibration isolation and mitigation device became a VE damper by removing the oblique springs and dampers. Hence, by letting $\zeta_h = 0$ and $\alpha = 0$, Eq. (13) became the dynamic equation of the system only with a VE damper. Similarly, the displacement transmissibility of the system can be obtained.

The absolute displacement transmissibility curves of the proposed device and the VE damper for different parameters are shown in Fig. 12. The initial isolation frequencies of the proposed device are significantly lower than those of the VE damper. For example, when the fractional order is 0.5, the initial isolation frequency reduces from 1.533 to 0.6104 by

Table 1. The parameters of the dynamic responses and displacement transmissibility analysis.

Case	Fractional order p	Displacement amplitude $\hat{Y}_0$	Horizontal damping ratio ζ_h	Vertical damping ratio ζ_v	Stiffness ratio α and structure parameter e_l
1	0.3, 0.5, 0.8, 1.0	0.1	0.05	0.1	0.75 and 0.6
2	0.5	0.05, 0.10, 0.15, 0.20	0.05	0.1	0.75 and 0.6
3	0.5	0.1	0.02, 0.05, 0.10, 0.12	0.1	0.75 and 0.6
4	0.5	0.1	0.05	0.02, 0.05, 0.10, 0.15	0.75 and 0.6
5	0.5	0.1	0.05	0.1	0.2143 and 0.3, 0.5 and 0.5, 0.75 and 0.6, 2 and 0.8

60.18%. When the fractional order is 1.0, the initial isolation frequency reduces from 1.424 to 0.2209 by 84.49%. Additionally, the peak values of the resonance region of the proposed device are also much lower than those of the VE damper. This indicates that the VE low-frequency visitation isolation and mitigation device can effectively reduce the initial isolation frequency and the peak value of resonance, and the vibration isolation performance in the low-frequency region is significantly better than those of the VE damper. It is because the stiffness of the proposed device with a negative stiffness structure is small, so the damping ratio is high, which leads to a lower resonance frequency and resonance response.

To investigate the effects of parameters on the vibration isolation performance of the proposed device, the absolute displacement transmissibility curves of the proposed device for different parameters are plotted in Fig. 13. The parameters used in the analysis are the same as those used in Section 3.2.2 and are shown in Table 1.

In Fig. 13(a), it is evident that as the fractional order increases, the initial isolation frequency decreases, the peak value in the resonance region decreases significantly, and the high-frequency transmissibility increases slightly. The initial isolation frequency reduces from 0.7119 to 0.2209, as the fractional order increases from 0.3 to 1.0. Meanwhile, the jump phenomenon of the absolute displacement transmissibility curve almost disappears when the fractional order is large.

In Fig. 13(b), the effects of the excitation amplitude on the transmissibility are shown. As the excitation amplitude increases, the initial isolation frequency increases and the transmissibility in the resonance region also increases significantly. The initial isolation frequency increases from 0.4667 to 1.02 when the fractional order increases from 0.05 to 0.2. This result is different from that of the linear vibration isolator, where the transmissibility is not affected by the excitation amplitude. To ensure better vibration isolation performance at low frequency, it was necessary to limit the usage scenario for the device, especially for the excitation amplitude.

Figures 13(c) and (d) illustrate the effects of horizontal and vertical damping on the transmissibility, respectively. Increasing horizontal damping results in a significant decrease in the peak value of displacement transmissibility in the resonance region, while it has little impact on the initial isolation frequency and high-frequency transmissibility. Vertical damping has a notable effect on absolute displacement transmissibility. As vertical damping increases, the initial isolation frequency increases and the peak value of transmissibility in the resonance region decreases significantly. For instance, as the vertical damping ratio increases from 0.02 to 0.15, the initial isolation frequency increases from 0.4837 to 0.7 by 44.78%.

Figure 13(e) shows the effects of the stiffness ratio α and structure parameter e_l on the transmissibility. It is evident that different combinations of α and e_l values have a significant effect on transmissibility. As e_l increases, the initial isolation frequency and the peak value of the transmissibility in the resonance region decrease first and then increase. Therefore, it is important to select a reasonable combination of α and e_l to achieve better vibration isolation performance for the device.

4.2. Time Responses to Harmonic Excitations

To verify the vibration isolation capability of the proposed device more intuitively, time history responses of the absolute displacement are analyzed. Moreover, time history responses of the VE damper (the vibration isolation device without oblique springs and dampers) are also simulated for comparison with those of the VE low-frequence vibration isolation and mitigation device. The simulations are carried out under the harmonic vibration excitation with fixed displacement amplitude and different excitation frequencies, as shown in Table 2. The parameters of the vibration isolation system are set as follows: $M = 10.6$ kg, $k_v = 420$ N/m, $k_h = 315$ N/m, $L = 50$ mm, $\zeta_h = 0.05$, $\zeta_v = 0.10$, $p = 0.5$. The absolute displacement responses of the two devices are shown in Fig. 14.

It can be seen from Fig. 14 that the displacement responses are slightly amplified in the low-frequency region for the proposed device due to the resonance effect. For example, when the excitation frequency is 0.1 Hz and 0.2 Hz, the displacement amplitude of the isolated object increases from 5 mm to 6.55 mm and 6.125 mm, respectively. The displacement amplitude of the object isolated by the proposed device is also slightly larger than that isolated by the VE damper. When the excitation frequency further increases, the displacement amplitude of the object isolated by the proposed device decreases obviously and is less than the excitation displacement amplitude. For example, when the excitation frequency is 0.5 Hz, the displacement amplitude decreases from 5 mm to 1.33 mm by 73.4%, and the vibration isolation phenomenon occurs. On the contrary, the displacement amplitude of the object isolated by the VE damper increases from 5 mm to 6.57 mm by 31.40%, and the displacement response is still amplified. It shows that the initial isolation frequency of the proposed device is lower than that of the VE damper. This is because the stiffness of the proposed device is smaller than that of the VE damper. Under the excitation frequency of 1.0 Hz, the displacement amplitude of the object isolated by the proposed device further decreases from 5 mm to 0.44 by 91.20%. However, the displacement amplitude of the object isolated by the VE damper is significantly amplified and increases from 5 mm to 61.03 mm by 1120%. This is because the natural frequency of the vibration isolation system consisting of only the VE damper is about 1 Hz, and the system is in the resonance region. When the excitation frequency is 2.0 Hz, the displacement amplitude of the object isolated by the proposed device and the VE damper both

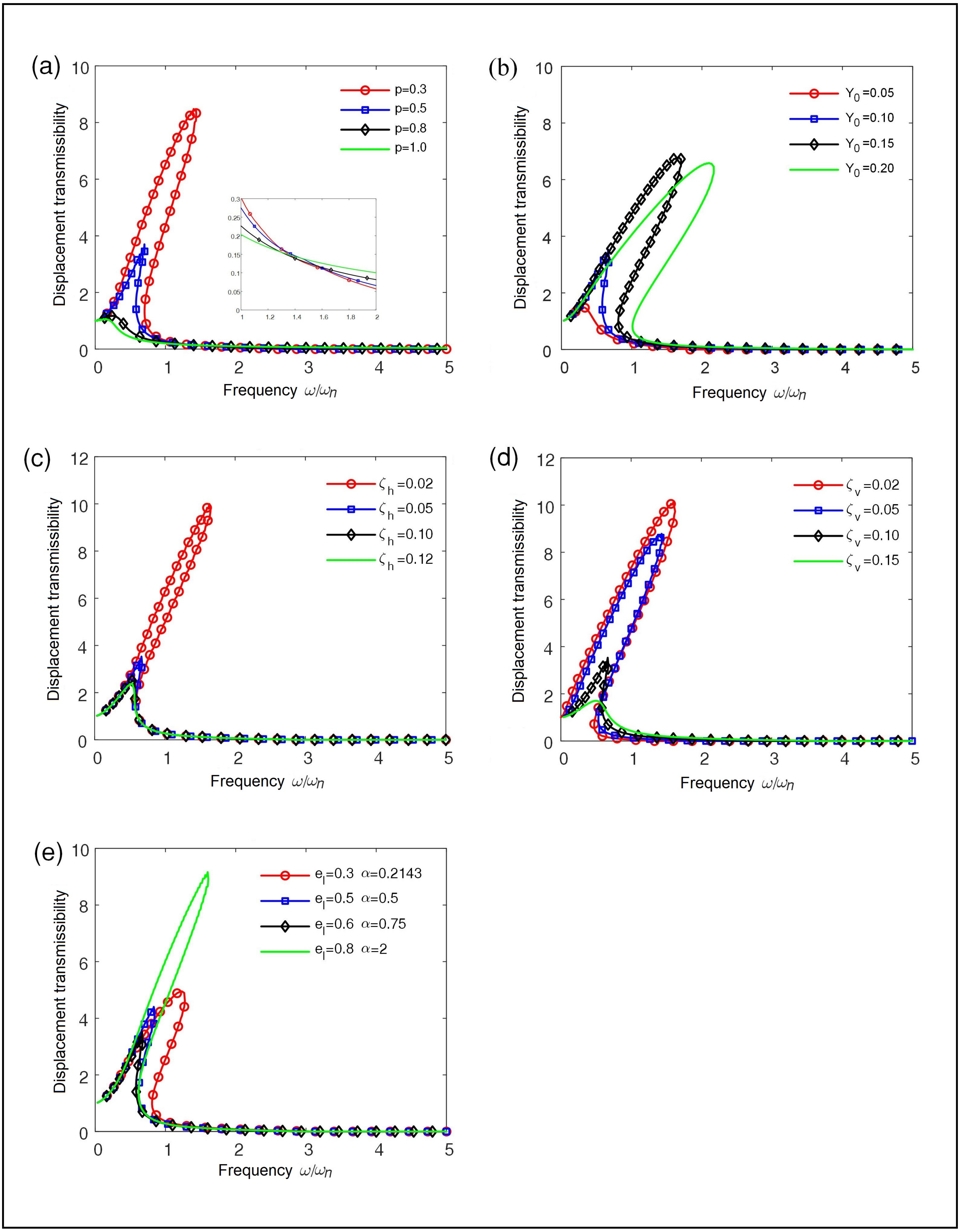

Figure 13. Effects of parameters on displacement transmissibility: (a) effects of fractional order, (b) effects of excitation amplitude, (c) effects of horizontal damping ratio, (d) effects of vertical damping ratio and (e) effects of stiffness ratio and structure parameter.

Table 2. The displacement amplitude of the proposed device and VE damper.

Displacement amplitude (mm)	Frequency (Hz)	The VE low-frequency vibration isolation and mitigation device		VE damper	
		Amplitude (mm)	Rate of change	Amplitude (mm)	Rate of change
5	0.1	6.55	31%	5.05	1%
	0.2	6.13	22.50%	5.2	3.90%
	0.5	1.33	73.40%	6.57	31.40%
	1	0.44	91.20%	61.03	1120%
	2	0.17	96.60%	1.87	62.60%

reduce, and the displacement amplitude of the object isolated by the proposed device reduces more significantly. To more clearly analyze the vibration isolation performance of the proposed device and the VE damper, the displacement amplitude and its variation of the isolated object are also listed in Table 2.

Therefore, the proposed VE low-frequency vibration isolation and mitigation device can effectively reduce the initial isolation frequency and broaden the isolation frequency interval.

5. CONCLUSIONS

This paper proposes a VE low-frequency vibration isolation and mitigation device by connecting a VE damper in parallel with two oblique springs and dampers. Firstly, the mechanical characteristics of the negative stiffness part consisting of two oblique springs and the positive stiffness part consisting of a VE damper are studied, respectively. Then, the effects of the system parameters on the stiffness displacement relationship and amplitude-frequency responses are discussed in detail. Finally, the vibration isolation performance of the VE low-frequency vibration isolation and mitigation device is evaluated by investigating the displacement transmissibility and time history responses. The main conclusions can be obtained as follows:

(1) Compared with the isolation device that only consists of a VE damper, the proposed VE low-frequency vibration isolation and mitigation device can effectively reduce the initial isolation frequency and broaden the isolation frequency interval.

(2) Horizontal damping is beneficial to improve the vibration isolation performance of the device, and the horizontal damper should be considered when the device is designed.

(3) The vibration isolation performance of the device is greatly affected by the excitation amplitude, and it can achieve excellent vibration isolation performance under the condition of small excitation amplitude.

(4) The mechanical parameters of the VE damper, such as the fractional order, the equivalent stiffness, and the equivalent damping have a great influence on the vibration isolation performance of the proposed device. Therefore, the VE material and the structure of the VE damper can be optimized to obtain more appropriate parameters to achieve excellent isolation performance of the device.

The system parameters significantly affect the proposed device's dynamic responses and vibration isolation performances. By selecting a reasonable combination of parameters, a device with good low-frequency isolation performance can be designed. This study is of great guiding significance for designing the low-frequency vibration isolation device. And future work can be focused on the experimental verification of the theoretical results.

ACKNOWLEDGEMENT

The authors gratefully acknowledge the financial support from Jiangsu Open University Fourteenth Five-Year Plan Project (2023XK019), Natural Science Foundation of the Jiangsu Higher Education Institutions of China (23KJB130003), National Natural Science Foundation of China (52178463), Shenzhen Sustainable Development Science and Technology Special Project (KCXFZ20211020165543004), National Key Research and Development Plans (2019YFE0121900), Jiangsu Provincial Natural Science Youth Fund Project (BK20230966), China Postdoctoral Science Foundation Special Support Project (2023TQ0105).

REFERENCES

[1] Yan, G., Zou, H.-X., Yan, H., Tan, T., Wang, S., Zhang, W.-M., Peng, Z.-K., and Meng, G. Multi-direction vibration isolator for momentum wheel assemblies, *ASME Journal of Vibration and Acoustics*, **142** (4), 041007, (2020). https://doi.org/10.1115/1.4046680

[2] Jiao, X., Zhang, J., Li, W., Wang, Y., Ma, W., and Zhao, Y. Advances in spacecraft micro-vibration suppression methods, *Progress in Aerospace Sciences*, **138**, 100898, (2023). https://doi.org/10.1016/j.paerosci.2023.100898

[3] Ning, D., Sun, S., Zhang, J., Du, H., Li, W., and Wang, X. An active seat suspension design for vibration control of heavy-duty vehicles, *Journal of Low Frequency Noise, Vibration and Active Control*, **35** (4), 264–278, (2016). https://doi.org/10.1177/0263092316676389

[4] Jing, X., Zhang, L., Feng, X., Sun, B., and Li, Q. A novel bio-inspired anti-vibration structure for operating hand-held jackhammers, *Mechanical Systems and Signal Processing*, **118**, 317–339, (2019). https://doi.org/10.1016/j.ymssp.2018.09.004

[5] Ghosh, T., and Sil, A. Effect of aspect ratio subjected to wind hazard in tall buildings situated along the coastal line of India, *The Structural Design of Tall and Special Buildings*, **31** (9), e1930, (2022). https://doi.org/10.1002/tal.1930

[6] Wang, L., Nagarajaiah, S., Shi, W., and Zhou, Y. Seismic performance improvement of base-isolated structures using a semi-active tuned mass damper, *Engineering Structures*, **271**, 114963, (2022). https://doi.org/10.1016/j.engstruct.2022.114963

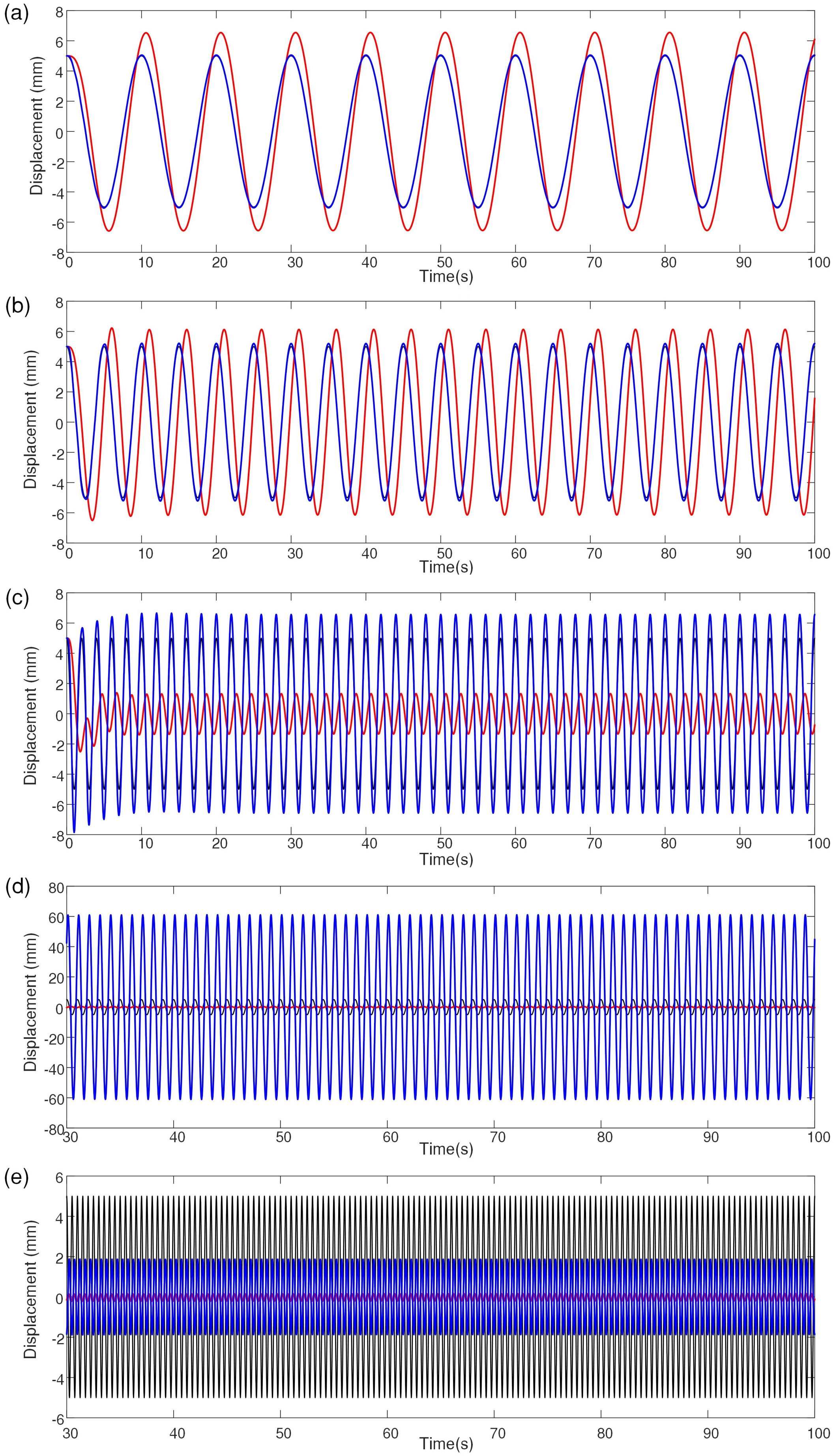

Figure 14. Displacement response with the proposed device (red line) and with the VE damper (blue line) under the base excitation (black line) at different excitation frequencies: (a) 0.1 Hz, (b) 0.2 Hz, (c) 0.5 Hz, (d) 1.0 Hz and (e) 2.0 Hz.

[7] Zhang, S. J., To, S., Zhang, G. Q., and Zhu, Z. W. A review of machine-tool vibration and its influence upon surface generation in ultra-precision machining, *International Journal of Machine Tools and Manufacture*, **91**, 34–42, (2015). https://doi.org/10.1016/j.ijmachtools.2015.01.005

[8] Ozsoy, M., Sims, N. D., and Ozturk, E. Robotically assisted active vibration control in milling: A feasibility study, *Mechanical Systems and Signal Processing*, **177**, 109152, (2022). https://doi.org/10.1016/j.ymssp.2022.109152

[9] Liu, C., Jing, X., Daley, S., and Li, F. Recent advances in micro-vibration isolation, *Mechanical Systems and Signal Processing*, **56**, 55–80, (2015). https://doi.org/10.1016/j.ymssp.2014.10.007

[10] Wani, Z. R., Tantray, M., Farsangi, E. N., Nikitas, N., Noori, M., Samali, B., and Yang, T. Y. A critical review on control strategies for structural vibration control, *Annual Reviews in Control*, **54**, 103–124, (2022). https://doi.org/10.1016/j.arcontrol.2022.09.002

[11] Luo, H., Fan, C., Li, Y., Liu, G., and Yu, C. Design and experiment of micro-vibration isolation system for optical satellite, *European Journal of Mechanics — A/Solids*, **97**, 104833, (2023). https://doi.org/10.1016/j.euromechsol.2022.104833

[12] Ledezma-Ramírez, D. F., Tapia-González, P. E., Ferguson, N., Brennan, M., and Tang, B. Recent advances in shock vibration isolation: an overview and future possibilities, *ASME Applied Mechanics Reviews*, **71** (6), 060802, (2019). https://doi.org/10.1115/1.4044190

[13] Wang, L., Zhao, Y., Sang, T., Zhou, H., Wang, P., and Zhao, C. Ultra-low frequency vibration control of urban rail transit: the general quasi-zero-stiffness vibration isolator, *Vehicle System Dynamics*, **60** (5), 1788–1805, (2022). https://doi.org/10.1080/00423114.2021.1874428

[14] Ma, Z., Zhou, R., and Yang, Q. Recent advances in quasi-zero stiffness vibration isolation systems: an overview and future possibilities, *Machines*, **10** (9), 813, (2022). https://doi.org/10.3390/machines10090813

[15] Liu, C., Zhang, W., Yu, K., Liu, T., and Zheng, Y. Quasi-zero-stiffness vibration isolation: Designs, improvements and applications, *Engineering Structures*, **301**, 117282, (2024). https://doi.org/10.1016/j.engstruct.2023.117282

[16] Wang, X., Liu, H., Chen, Y., and Gao, P. Beneficial stiffness design of a high-static-low-dynamic-stiffness vibration isolator based on static and dynamic analysis, *International Journal of Mechanical Sciences*, **142**, 235–244, (2018). https://doi.org/10.1016/j.ijmecsci.2018.04.053

[17] Zhou, J., Wang, X., Xu, D., and Bishop, S. Nonlinear dynamic characteristics of a quasi-zero stiffness vibration isolator with cam–roller–spring mechanisms, *Journal of Sound and Vibration*, **346**, 53–69, (2015). https://doi.org/10.1016/j.jsv.2015.02.005

[18] Zhou, J., Xu, D., and Bishop, S. A torsion quasi-zero stiffness vibration isolator, *Journal of Sound and Vibration*, **338**, 121–133, (2015). https://doi.org/10.1016/j.jsv.2014.10.027

[19] Zhou, J., Xiao, Q., Xu, D., Ouyang, H., and Li, Y. A novel quasi-zero-stiffness strut and its applications in six-degree-of-freedom vibration isolation platform, *Journal of Sound and Vibration*, **394**, 59–74, (2017). https://doi.org/10.1016/j.jsv.2017.01.021

[20] Lian, X., Deng, H., Han, G., Jiang, F., Zhu, L., Shao, M., Liu, X., Hu, R., Gao, Y., and Ma, M. A low-frequency micro-vibration absorber based on a designable quasi-zero stiffness beam, *Aerospace Science and Technology*, **132**, 108044, (2023). https://doi.org/10.1016/j.ast.2022.108044

[21] Wu, J., Zeng, L., Han, B., Zhou, Y., Luo, X., Li, X., Chen, X., and Jiang, W. Analysis and design of a novel arrayed magnetic spring with high negative stiffness for low-frequency vibration isolation, *International Journal of Mechanical Sciences*, **216**, 106980, (2022). https://doi.org/10.1016/j.ijmecsci.2021.106980

[22] Yan, G., Wang, S., Zou, H., Zhao, L., Gao, Q., and Zhang, W. Bio-inspired polygonal skeleton structure for vibration isolation: Design, modelling, and experiment, *Science China Technological Sciences*, **63** (12), 2617–2630, (2020). https://doi.org/10.1007/s11431-020-1568-8

[23] Yan, G., Qi, W.-H., Shi, J.-W., Yan, H., Zou, H.-X., Zhao, L.-C., Wu, Z.-Y., Fang, X.-Y., Li, X.-Y., and Zhang, W.-M. Bionic paw-inspired structure for vibration isolation with novel nonlinear compensation mechanism, *Journal of Sound and Vibration*, **525**, 116799, (2022). https://doi.org/10.1016/j.jsv.2022.116799

[24] Yan, G., Zou, H.-X., Wang, S., Zhao, L.-C., Wu, Z.-Y., and Zhang, W.-M. Bio-inspired toe-like structure for low-frequency vibration isolation, *Mechanical Systems and Signal Processing*, **162**, 108010, (2022). https://doi.org/10.1016/j.ymssp.2021.108010

[25] Zhao, F., Ji, J. C., Ye, K., and Luo, Q. Increase of quasi-zero stiffness region using two pairs of oblique springs, *Mechanical Systems and Signal Processing*, **144**, 106975, (2020). https://doi.org/10.1016/j.ymssp.2020.106975

[26] Zhao, F., Cao, S., Luo, Q., and Ji, J. Enhanced design of the quasi-zero stiffness vibration isolator with three pairs of oblique springs: theory and experiment, *Journal of Vibration and Control*, **29** (9–10), 2049–2063, (2023). https://doi.org/10.1177/10775463221074143

[27] Gatti, G., Ledezma-Ramirez, D. F., and Brennan, M. J. Performance of a shock isolator inspired by skeletal muscles, *International Journal of Mechanical Sciences*, **244**, 108066, (2023). https://doi.org/10.1016/j.ijmecsci.2022.108066

[28] Chen, T., Zheng, Y., Song, L., Gao, X., and Wang, G. Study on a quasi-zero-stiffness isolator for variable mass load, *Applied Mathematical Modelling*, **123**, 447–463, (2023). https://doi.org/10.1016/j.apm.2023.07.012

[29] Zheng, Y., Shangguan, W.-B., Yin, Z., and Liu, X.-A. Design and modeling of a quasi-zero stiffness isolator for different loads, *Mechanical Systems and Signal Processing*, **188**, 110017, (2023). https://doi.org/10.1016/j.ymssp.2022.110017

30 Guo, S., Gao, R., Tian, X., and Liu, S. A quasi-zero-stiffness elastic metamaterial for energy absorption and shock attenuation, *Engineering Structures*, **280**, 115687, (2023). https://doi.org/10.1016/j.engstruct.2023.115687

31 Ling, P., Miao, L., Ye, B., You, J., Zhang, W., and Yan, B. Ultra-low frequency vibration isolation of a novel click-beetle-inspired structure with large quasi-zero stiffness region, *Journal of Sound and Vibration*, **558**, 117756, (2023). https://doi.org/10.1016/j.jsv.2023.117756

32 Wang, Q., Zhou, J., Wang, K., Lin, Q., Xu, D., and Wen, G. A compact quasi-zero-stiffness device for vibration suppression and energy harvesting, *International Journal of Mechanical Sciences*, **250**, 108284, (2023). https://doi.org/10.1016/j.ijmecsci.2023.108284

33 Liu, Y., Xu, L., Song, C., Gu, H., and Ji, W. Dynamic characteristics of a quasi-zero stiffness vibration isolator with nonlinear stiffness and damping, *Archive of Applied Mechanics*, **89**, 1743–1759, (2019). https://doi.org/10.1007/s00419-019-01541-0

34 Mori, K., Kono, D., Yamaji, I., and Matsubara, A. Modelling of viscoelastic damper support for reduction in low frequency residual vibration in machine tools, *Precision Engineering*, **50**, 313–319, (2017). https://doi.org/10.1016/j.precisioneng.2017.06.004

35 Darabi, B., Rongong, J. A., and Zhang, T. Viscoelastic granular dampers under low-amplitude vibration, *Journal of Vibration and Control*, **24** (4), 708–721, (2018). https://doi.org/10.1177/1077546316650098

36 Xu, C., Xu, Z.-D., Huang, X.-H., Xu, Y.-S., and Ge, T. Modeling and analysis of a viscoelastic micro-vibration isolation and mitigation platform for spacecraft, *Journal of Vibration and Control*, **24** (18), 4337–4352, (2018). https://doi.org/10.1177/1077546317724321

37 Lewandowski, R. Influence of temperature on the dynamic characteristics of structures with viscoelastic dampers, *Journal of Structural Engineering*, **145** (2), 04018245, (2019). https://doi.org/10.1061/(ASCE)ST.1943-541X.0002238

38 Dong, Y.-R., Xu, Z.-D., Shi, Q., Li, Q.-Q., He, Z.-H., and Cheng, Y. Seismic performance and material-level damage evolution of retrofitted RC framed structures by high-performance AVED under different shear-span ratio, *Journal of Building Engineering*, **63**, 105495, (2023). https://doi.org/10.1016/j.jobe.2022.105495

39 Xu, C., Xu, Z.-D., Ge, T., and Liao, Y.-X. Modeling and experimentation of a viscoelastic microvibration damper based on a chain network model, *Journal of Mechanics of Materials and Structures*, **11** (4), 413–432, (2016). https://doi.org/10.2140/jomms.2016.11.413

40 Dai, J., Xu, Z.-D., and Gai, P.-P. Dynamic analysis of viscoelastic tuned mass damper system under harmonic excitation, *Journal of Vibration and Control*, **25** (11), 1768–1779, (2019). https://doi.org/10.1177/1077546319833887

41 Ge, T., Huang, X. H., Guo, Y. Q., He, Z. F., and Hu, Z. W. Investigation of mechanical and damping performances of cylindrical viscoelastic dampers in wide frequency range, *Actuators*, **10** (71), 1–15, (2021). https://doi.org/10.3390/act10040071

42 Shu, Z., You, R., and Zhou, Y. Viscoelastic materials for structural dampers: A review, *Construction and Building Materials*, **342**, 127955, (2022). https://doi.org/10.1016/j.conbuildmat.2022.127955

43 Liu, C., Tang, J., Yu, K., Liao, B., Hu, R., and Zang, X. On the characteristics of a quasi-zero-stiffness vibration isolator with viscoelastic damper, *Applied Mathematical Modelling*, **88**, 367–381, (2020). https://doi.org/10.1016/j.apm.2020.06.068

44 Xu, Z. D., Liao, Y. X., Ge, T., and Xu, C. Experimental and theoretical study of viscoelastic dampers with different matrix rubbers, *Journal of Engineering Mechanics*, **142** (8), 04016051, (2016). https://doi.org/10.1061/(ASCE)EM.1943-7889.0001101

45 Baz, A. M. *Active and passive vibration damping*, John Wiley and Sons, NY, (2019).

46 Pritz, T. Five-parameter fractional derivative model for polymeric damping materials, *Journal of Sound and Vibration*, **265** (5), 935-952, (2003). https://doi.org/10.1016/S0022-460X(02)01530-4

47 Xu, Y., Xu, Z.-D., Guo, Y.-Q., Ge, T., Xu, C., and Huang, X. Theoretical and experimental study of viscoelastic damper based on fractional derivative approach and micromolecular structures, *ASME Journal of Vibration and Acoustics*, **141** (3), 031010, (2019). https://doi.org/10.1115/1.4042517

48 Shen, Y., Yang, S., Xing, H., and Gao, G. Primary resonance of Duffing oscillator with fractional-order derivative, *Communications in Nonlinear Science and Numerical Simulation*, **17** (7), 3092–3100, (2012). https://doi.org/10.1016/j.cnsns.2011.11.024

49 Liu, Y., Ji, W., Deng, E., Wang, X., and Song, C. Dynamic characteristics of two degree-of-freedom quasi-zero stiffness vibration isolation system with nonlinear springs, *Mechanics Based Design of Structures and Machines*, **51** (6), 3100–3118, (2021). https://doi.org/10.1080/15397734.2021.1919142

50 Xue, D. *Fractional-order control systems: fundamentals and numerical implementations*, Walter de Gruyter GmbH & Co KG, (2017).